State-to-state reaction probabilities using bond coordinates: Application to the Li+HF(v,j) collision

Manuel Lara, Alfredo Aguado, Miguel Paniagua, and Octavio Roncero

Citation: J. Chem. Phys. **113**, 1781 (2000); doi: 10.1063/1.481982
View online: http://dx.doi.org/10.1063/1.481982
View Table of Contents: http://jcp.aip.org/resource/1/JCPSA6/v113/i5
Published by the American Institute of Physics.

State-to-state reaction probabilities using bond coordinates: Application to the Li+HF(v,j) collision

Manuel Lara, Alfredo Aguado, and Miguel Paniagua
Departamento de Química Física, Facultad de Ciencias C-XIV, Universidad Autónoma de Madrid, 28049 Madrid, Spain

Octavio Roncero
Instituto de Matemáticas y Física Fundamental, C.S.I.C., Serrano 123, 28006 Madrid, Spain

(Received 23 November 1999; accepted 1 May 2000)

In this work we present a time-dependent method to evaluate state-to-state reaction probabilities, based on bond coordinates and an adapted body-fixed frame. Such a method is expected to be rather efficient to describe $A+BC\rightarrow AB+C$ reactive collisions. In addition, the apparent complexity of the Hamiltonian expressed in these coordinates is reduced when applied to a wave packet represented in grids for the internal coordinates. The efficiency of this method as compared to the use of the most adapted Jacobi coordinates increases as the masses of the satellite atoms approach that of the heavier central atom and, what may be more important, avoids the problems associated with the singularities of the radial kinetic terms in the region of configuration space of interest. This method is used to study the Li+HF($v=0,1,j=0,J=0$) reactive collision and the structure of the final state distribution of the LiF products is interpreted in terms of transition state resonances. © *2000 American Institute of Physics.* [S0021-9606(00)00629-2]

I. INTRODUCTION

The field of molecular reaction dynamics has undergone a great development during the last decade. For some gas phase bimolecular reactions, a deep description on a molecular level is starting to be possible.[1] Both theoretical methodologies[2] and experimental techniques[3] allow nowadays, at least for very simple systems, the calculation and measurement of interesting quantities such as state-specific differential cross sections.[4] Moreover, there is a growing interest in the field of the stereodynamics and vector correlations since the associated magnitudes provide the most detailed information about chemical reactions and their anisotropic character.[5–12] Recently, Miranda and Clary[13] have proposed a complete quantum treatment for the study of vector properties in reactive collisions, that has been applied to describe the stereodynamics of the $H+D_2$ reactive collisions.[14,15] Such quantum treatments, however, require the calculation of the collision *S*-matrix and hence of the state-to-state reaction probabilities.

Methods to accurately calculate the *S*-matrix for reactive collisions are traditionally classified as time-independent (TI) or time-dependent (TD),[2,16] each one having its own advantages and disadvantages. Among the TI methods the most widely used ones are the close-coupling hyperspherical method,[17–26] and the variational principle methods.[27–31] An interesting technique is the use of negative imaginary potentials (NIPS) either for TI[32] or for TD treatments.[33] In particular, the use of NIPS, together with some analogous absorbing techniques,[34–37] have produced a rapid development of TD methods since it allows to reduce the numerical integration of the time-dependent Schrödinger equation to the interaction region, eliminating the asymptotic regions where the propagation can be continued analytically.[36] The *S*-matrix can be then calculated at the edge of the asymptotic region using different methods.[38–43]

The asymptotic solutions required to extract the *S*-matrix can be written in a simple separable way using the Jacobi coordinates associated to each arrangement channel.[44] That is the reason why the study of the reaction dynamics with wave packets is usually performed in reactant Jacobi coordinates. Combining the use of NIPS[33] with the evaluation of the flux to products[45] it is possible to obtain total reaction probabilities in a rather efficient manner without the necessity of describing the product asymptotic region. The evaluation of state-to-state reaction probabilities requires the description of the dynamics up to the product asymptotic region. Reactant Jacobi coordinates have been used in some cases as $H+H_2$[46] and $H+O_2$[43] collisions, but usually describe very poorly the product asymptotic regions (many grid points would be required). In order to impose the proper product asymptotic conditions the wave packet should be transformed to product Jacobi coordinates at each time step. Another similar alternative is to transform only the initial wave packet from reactant to product Jacobi coordinates, and to perform the time propagation in this last set of coordinates. However, this still requires dense grids and only few cases have been studied as the prototypical case $H+H_2$ and isotopic variants.[46,47] In general, the particular set of Jacobi coordinates to be used in the propagation will depend on the system under study.[46] In spite of its difficulty, some tetraatomic benchmark examples of time-dependent methods using a single set of Jacobi coordinates to extract state-to-state information are the $H+H_2O\rightarrow H_2+OH$ collisions[48] and the reverse reaction.[49]

In order to obtain the state-to-state reaction probabilities more efficiently some refined methods have been proposed.

One is to initialize the propagation in reactant Jacobi coordinates until the wave packet is in the interaction region and, then, transform it to product Jacobi coordinates in which the propagation is continued and the required *S*-matrix elements obtained.[50–52] This method allows us to split the problem in two, using the set of Jacobi coordinates more appropriate in each region, and was first proposed by Judson *et al.*[50] to study $H+H_2$ collisions and afterwards applied to Li+HF by Gögtas *et al.*[52] The approach presents some difficulties as far as the wave packet spreads over a large portion of the configuration space,[46] as it happens for long range interaction potentials in the entrance channel, and in the presence of long lived resonances. In such situations the wave packet to be transformed may be spread in a quite large region and, therefore, both reactant and product regions need to be properly described.

More recently, Zhang and co-workers proposed the reactant-product decoupling (RPD) method[53–55] also applied in the time-independent domain.[56] The wave packet is split in several parts, each of them essentially confined to a single arrangement channel. These different parts are connected through imaginary potentials, which act as sinks and sources to transfer from one region to another, and avoid reflections at the edges of the grids. This formalism, essentially rigorous, has the advantage of describing the dynamics in the most adapted set of Jacobi coordinates but present some problems. First, the portion of the wave packet to be transferred has to be transformed at each time step from one set of Jacobi coordinates to another, what may be computationally expensive. Second, the portions transferred are affected by the imaginary potentials, what can reduce the accuracy of the procedure.

In treating high total angular momenta using a body-fixed frame, the number of helicity functions is usually limited in order to make the calculation feasible. The change of body-fixed frame along the propagation would require the inclusion of a large number of helicity functions in the less adapted frame. In order to describe reactant and product regions well enough at the same time, new sets of coordinates can be designed. The state-to-state reaction probability can then be extracted at the asymptotic region through a transformation to the corresponding Jacobi coordinates, without affecting the accuracy of the propagation or the actual number of helicity functions included in the propagation. The most used set of such coordinates are the hyperspherical ones, specially for time independent calculation. However, there are only few full time-dependent calculation on reactive scattering reported in the literature.[57,58] Using hyperspherical coordinates has the difficulty that for a moderately large hyper-radius many grid points, or equivalently many basis functions, are required to describe the hyperangles. Such a problem is overcome in time-independent calculations by the use of the so-called diabatic-by-sector method.[59] However, the use of that method in time dependent calculation would be very inefficient.

In this work we propose, as an alternative, to use bond coordinates for the internal degrees of freedom, i.e., R_{AB}, R_{BC} and the angle α between them, to describe the reactive collisions where only two arrangement channels are of interest, $A+BC \rightarrow AB+C$, while the third channel (correlating to *AC* fragments) either is energetically closed or not of interest. These coordinates describe correctly the transition state region and are able to reasonably describe relatively long distances, especially when the central *B* atom is much heavier than *A* and *C*. This method, presented in Sec. II, is applied in Sec. III to the study of Li+HF reactive collisions, to form LiF products (the LiH channel is closed at the energies of interest). LiHF is particularly well suited to be studied using these coordinates because the central F atom is the heaviest one of the system. Due to the relatively light atoms involved in the Li+HF reaction, the system is becoming a benchmark and there are several global potential energy surfaces[60,61] (GPES) and an increasing number of quantum dynamical studies on the reactive collision.[52,60–65] Also, the efficiency using bond coordinates is compared with that of different sets of Jacobi coordinates for LiHF and its isotopomers.

II. THE METHOD

A. Coordinates and Hamiltonian

It is convenient to use a body-fixed frame which allows to distinguish between internal coordinates, describing the relative location of the atoms, and three Euler angles (θ, ϕ, and χ), specifying the orientation of the body-fixed axis with respect to the space-fixed frame. In this case, we shall consider that the three atoms are in the $x-z$ body-fixed plane, and the *z*-axis lies along the vector joining the center of mass of the *AB* diatomic reagent (HF in this case) to the *C* atom (see Fig. 1), i.e., along the reactant Jacobi vector **R**. Such an election of the body-fixed frame is made for two reasons. First, the *z*-axis of this frame is parallel to the relative velocity between the reactants, **k**, in the asymptotic region and, therefore, is the direction of experimental significance and all other vector magnitudes can be referred to it. Second, in a previous work on the Li+HF collision[61] with the same body-fixed frame, total reaction probabilities for $J=5$ total angular momentum, using the centrifugal sudden (CS) approximation were found to be in rather good agreement with an exact calculation. It was concluded that Ω, the projection of the total angular momentum on this *z*-body fixed frame, is reasonably well conserved in the entrance channel, at least for low *J*, because the H atom is very light as compared to F and Li atoms, so that the HF fragment behaves as a pseudo-atom. However, nothing can be said about the dynamics in the product valley where this frame may not be well adapted. In any case, this election of the body-fixed frame is expected to yield a rapid convergence on the sum over Ω.

The internal coordinates used to describe the relative position of the nuclei are bond coordinates: R_1, the FH internuclear distance in the present case, R_2, the FLi internuclear distance, and the angle, α, between the associated vectors (see Fig. 1). Being the central F atom much heavier ($m_0 \approx 19$ amu) as compared to H ($m_1 \approx 1$ amu) and Li ($m_2 \approx 7$ amu), these coordinates are quite similar to both reactant and product Jacobi coordinates, describing Li+HF and H+LiF arrangements, respectively. It is therefore expected that near the asymptotic regions, the dynamics can be de-

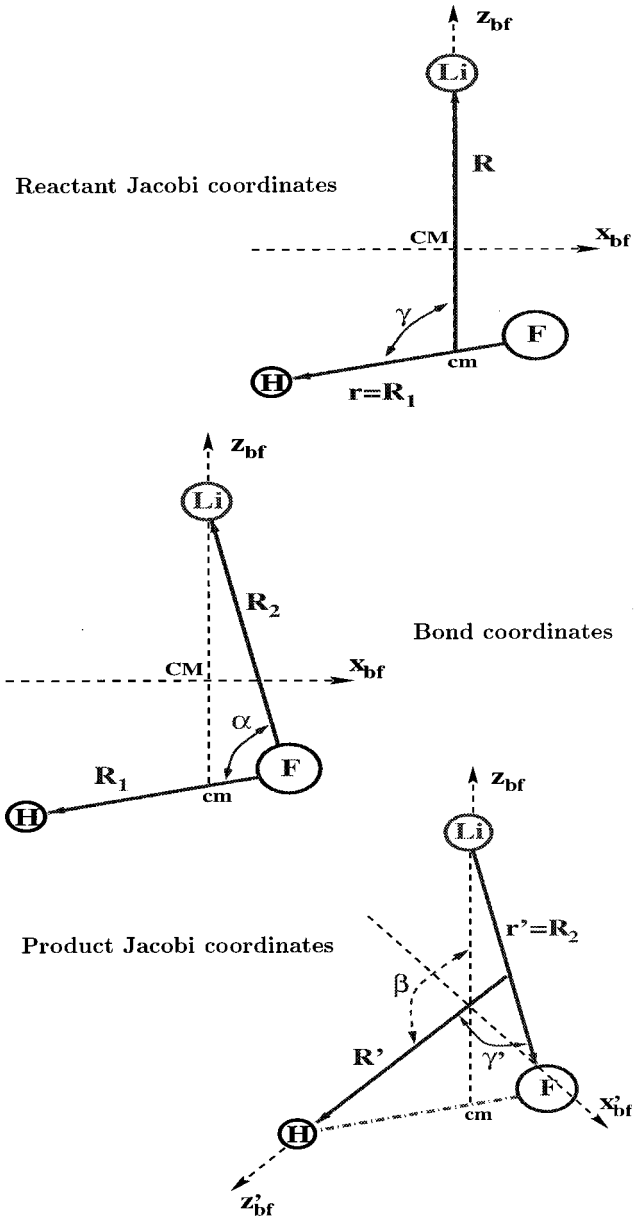

FIG. 1. Systems of internal coordinates and associated body-fixed frames used in the method.

scribed quite efficiently using these coordinates.

Expressed in this system of coordinates $(\theta,\phi,\chi,R_1,R_2,\alpha)$, the Hamiltonian takes the form

$$H=-\frac{\hbar^2}{2\mu_1}\left(\frac{1}{R_1^2}\frac{\partial}{\partial R_1}R_1^2\frac{\partial}{\partial R_1}\right)-\frac{\hbar^2}{2\mu_2}\left(\frac{1}{R_2^2}\frac{\partial}{\partial R_2}R_2^2\frac{\partial}{\partial R_2}\right)+\left(\frac{1}{2\mu_1R_1^2}+\frac{1}{2\mu_2R_2^2}\right)\hat{\mathbf{L}}^2+\frac{(\hat{\mathbf{J}}^2-2\hat{\mathbf{J}}\cdot\hat{\mathbf{j}})}{2\mu R^2}+\hat{T}_{12}+V(R_1,R_2,\alpha), \tag{1}$$

where $\mu_1=m_0m_1/(m_0+m_1)$, $\mu_2=m_0m_2/(m_0+m_2)$ are the reduced masses associated with $\mathbf{R_1}$ and $\mathbf{R_2}$, while $\mu=m_2(m_0+m_1)/(m_0+m_1+m_2)$ is the reduced mass associated with the $\mathbf{R}$ Jacobi vector. The volume element is given by $R_1^2dR_1R_2^2dR_2\sin\alpha d\alpha\sin\theta d\theta d\phi d\chi$.

In Eq. (1), $\hat{\mathbf{L}}^2$ is the angular momentum operator appearing in this set of internal coordinates

$$\hat{\mathbf{L}}^2=-\hbar^2\left\{\frac{1}{\sin\alpha}\frac{\partial}{\partial\alpha}\sin\alpha\frac{\partial}{\partial\alpha}+\frac{1}{\sin^2\alpha}\frac{\partial^2}{\partial\chi^2}\right\}. \tag{2}$$

$\hat{\mathbf{J}}$ is the total angular momentum of the system given by

$$\hat{\mathbf{J}}^2=-\hbar^2\left\{\frac{\partial^2}{\partial\theta^2}+\cot\theta\frac{\partial}{\partial\theta}+\frac{1}{\sin^2\theta}\times\left(\frac{\partial^2}{\partial\phi^2}+\frac{\partial^2}{\partial\chi^2}-2\cos\theta\frac{\partial^2}{\partial\chi\partial\phi}\right)\right\},$$

$$\hat{J}_x=-i\hbar\left\{\cos\chi\cot\theta\frac{\partial}{\partial\chi}-\frac{\cos\chi}{\sin\theta}\frac{\partial}{\partial\phi}+\sin\chi\frac{\partial}{\partial\theta}\right\},$$

$$\hat{J}_y=-i\hbar\left\{-\sin\chi\cot\theta\frac{\partial}{\partial\chi}+\frac{\sin\chi}{\sin\theta}\frac{\partial}{\partial\phi}+\cos\chi\frac{\partial}{\partial\theta}\right\},$$

$$\hat{J}_z=-i\hbar\frac{\partial}{\partial\chi}. \tag{3}$$

The term $(\hat{\mathbf{J}}^2-2\hat{\mathbf{J}}\cdot\hat{\mathbf{j}})/2\mu R^2$ ($\hat{\mathbf{j}}$ is the angular momentum operator associated with the diatomic fragment in reactant Jacobi coordinates) arises from the use of the Jacobi body-fixed frame (the missing $\hat{\mathbf{j}}^2/2\mu R^2$ term appearing in Jacobi coordinates has been incorporated in the term containing $\hat{\mathbf{L}}^2$). $\hat{\mathbf{J}}\cdot\hat{\mathbf{j}}$ is responsible for the Coriolis coupling and is written as

$$\hat{\mathbf{J}}\cdot\hat{\mathbf{j}}=-i\hbar\left\{\left(\frac{qR_1}{R_2\sin\alpha}-\cot\alpha\right)\hat{J}_x\frac{\partial}{\partial\chi}-qR_1\sin\alpha\hat{J}_y\times\frac{\partial}{\partial R_2}+\left(1-\frac{qR_1\cos\alpha}{R_2}\right)\hat{J}_y\frac{\partial}{\partial\alpha}+\hat{J}_z\frac{\partial}{\partial\chi}\right\}, \tag{4}$$

where $q=\mu_1/m_0$ (with $R^2=R_2^2+q^2R_1^2-2qR_1R_2\cos\alpha$).

Finally, in Eq. (1) $\hat{T}_{12}$ is the kinetic crossing term due to the non-Jacobian character of the internal coordinates chosen and has the form

$$\hat{T}_{12}=\frac{\hbar^2}{m_0}\left\{\frac{\sin\alpha}{R_1R_2}\frac{\partial}{\partial\alpha}-\cos\alpha\frac{\partial^2}{\partial R_1\partial R_2}+\frac{\sin\alpha}{R_2}\frac{\partial^2}{\partial R_1\partial\alpha}+\frac{\sin\alpha}{R_1}\frac{\partial^2}{\partial R_2\partial\alpha}\right\}-\frac{\cos\alpha}{m_0R_1R_2}\hat{\mathbf{L}}^2. \tag{5}$$

This Hamiltonian is analogous to some previously derived ones for this kind of coordinates[66–72] but using, in general, a different body-fixed frame. Thus, the Hamiltonian for $J=0$ in Eq. (1) is the same as those previously reported.[66–72] This kind of coordinates has been generally used for the calculation of rovibrational states of triatomic systems.[66,67] The dynamics, however, has only been scarcely studied exactly using this kind of coordinates in three dimensions. This is possibly due to the difficulty introduced by the kinetic crossing term, which is non-negligible even at asymptotic distances.

B. Wave packet representation and propagation

The total wave packet is expanded as

$$\Psi^{JMp}(\theta,\phi,\chi,R_1,R_2,\alpha,t) = \sum_{\Omega\geqslant 0}^{J} W^{Jp}_{M\Omega}(\phi,\theta,\chi)\frac{\Phi^{JMp}_{\Omega}(R_1,R_2,\alpha,t)}{R_1R_2}, \tag{6}$$

where $W^{Jp}_{M\Omega}$ are linear combinations of Wigner rotation matrices[73] such that the parity under inversion of all coordinates, p, is well defined

$$W^{Jp}_{M\Omega}(\phi,\theta,\chi) = \sqrt{\frac{2J+1}{16\pi^2(1+\delta_{\Omega,0})}}[D^{J*}_{M,\Omega}(\phi,\theta,\chi) + p(-1)^{J+\Omega}D^{J*}_{M,-\Omega}(\phi,\theta,\chi)], \tag{7}$$

M and Ω being the quantum numbers for the projections of the total angular momentum, J, on the space-fixed and body fixed z-axis, respectively. Insertion of Eq. (6) into the time-dependent Schrödinger equation using the Hamiltonian, Eq. (1), yields a set of first order differential equations for the $\Phi^{JMp}_{\Omega}(R_1,R_2,\alpha,t)$ coefficients,

$$\begin{aligned} i\hbar\frac{\partial\Phi^{JMp}_{\Omega}}{\partial t} = \Bigg\{ & -\frac{\hbar^2}{2\mu_1}\frac{\partial^2}{\partial R_1^2} - \frac{\hbar^2}{2\mu_2}\frac{\partial^2}{\partial R_2^2} \\ & + \left(\frac{1}{2\mu_1R_1^2}+\frac{1}{2\mu_2R_2^2}\right)\hat{\mathbf{l}}^2 \\ & + \hbar^2\frac{J(J+1)-2\Omega^2}{2\mu R^2} + \hat{t}_{12} + V\Bigg\}\Phi^{JMp}_{\Omega} \\ & + \sum_{\Omega'}\delta_{\Omega'\Omega\pm 1}\frac{\hbar^2\hat{t}_c}{2\mu R^2}\sqrt{J(J+1)-\Omega\Omega'} \\ & \times\sqrt{1+\delta_{\Omega,0}}\sqrt{1+\delta_{\Omega',0}}\Phi^{JMp}_{\Omega'}, \end{aligned} \tag{8}$$

with the following substitutions:

$$\begin{aligned} \hat{\mathbf{l}}^2 &= -\hbar^2\left(\frac{1}{\sin\alpha}\frac{\partial}{\partial\alpha}\sin\alpha\frac{\partial}{\partial\alpha} - \frac{\Omega^2}{\sin^2\alpha}\right), \\ \hat{t}_c &= \Omega'\left(\cot\alpha - \frac{qR_1}{R_2\sin\alpha}\right) \pm \Bigg[-qR_1\sin\alpha\frac{\partial}{\partial R_2} \\ &\quad + q\frac{R_1}{R_2}\sin\alpha + \left(1-q\frac{R_1}{R_2}\cos\alpha\right)\frac{\partial}{\partial\alpha}\Bigg], \\ \hat{t}_{12} &= \frac{\hbar^2}{m_0}\Bigg[\sin\alpha\frac{\partial}{\partial\alpha}\left(\frac{1}{R_1}\frac{\partial}{\partial R_2}+\frac{1}{R_2}\frac{\partial}{\partial R_1}-\frac{1}{R_1R_2}\right) \\ &\quad + \cos\alpha\left(\frac{1}{R_1}\frac{\partial}{\partial R_2}+\frac{1}{R_2}\frac{\partial}{\partial R_1}-\frac{1}{R_1R_2}-\frac{\partial^2}{\partial R_1\partial R_2}\right)\Bigg] \\ &\quad - \frac{\cos\alpha}{m_0R_1R_2}\hat{\mathbf{l}}^2. \end{aligned} \tag{9}$$

The integration of the above equations is performed using the Chebyshev method[74] and the $\Phi^{JMp}_{\Omega}(R_1,R_2,\alpha,t)$ coefficients are represented on finite grids for the internal coordinates R_1,R_2,α. A set of equidistant points, R_1^i,R_2^j, is chosen for the rectangular bidimensional radial grid $(n_1\times n_2)$.

TABLE I. Parameters used in the wave packet propagations for $v=0,1$, $j=0$, $J=0$.

	$v=0$, $j=0$	$v=1$, $j=0$
$[R_1^{\min}(\text{Å}), R_1^{\max}(\text{Å})\ n_1]$	0.25, 18.87, 448	0.60, 18.93, 440
$[R_2^{\min}(\text{Å}), R_2^{\max}(\text{Å}), n_2]$	0.50, 20.82, 480	1.12, 19.89, 462
n_α	32	40
$[R_1^{\text{abs}}(\text{Å}), \gamma_1]$	14.00, 0.015	14.00, 0.012
$[R_2^{\text{abs}}(\text{Å}), \gamma_2]$	14.50, 0.020	14.50, 0.016
$[R_0(\text{Å}), \mathcal{K}_0, \Gamma]$	13.00, 22.02, 0.27	13.00, 22.02, 0.27
$\Delta t(\text{ps}), t_{\max}(\text{ps})$	0.004, 8.68	0.002, 3.99
$R'_\alpha(\text{Å})$	13.00	13.00

For the angle α a set of n_α Gauss–Legendre quadrature points, α^k (with weights ω^k), is used. The grid representation of the wave packet is then given by

$$[\Phi^{JMp}_{\Omega}]_{ijk} = \Phi^{JMp}_{\Omega}(R_1^i,R_2^j,\alpha^k)\sqrt{\omega^k}. \tag{10}$$

In order to use a finite bidimensional radial grid, the wave packet is absorbed at each time step by multiplying the wave packet by $f_1(R_1)f_2(R_2)$, where $f_i(R_i)=\exp[-\gamma_i(R_i-R_i^{\text{abs}})^2]$ for $R_i>R_i^{\text{abs}}$ and $f_i(R_i)=1$ otherwise. The actual parameters of the propagation used for the calculations are listed in Table I.

The size of the grid can be further reduced using the L-shape method of Mowrey[75] which can be considered the grid analogous to the asymptotic-interaction separation approaches of Neuhauser *et al.*[51] and Zhang and Zhang.[76] The radial grid points kept in the calculations are those for which the potential is lower than a given criterium for all the angles. The criterium is chosen according to the energy content of the wave packet so that points which are not energetically accessible are omitted. Such procedure allows to eliminate in the actual calculation the region of the configuration space corresponding to the three separated atoms, and the remaining domain of the configuration space is L-shaped,[75] thus obtaining substantial savings in memory requirements and computing time. The radial kinetic terms are evaluated using fast Fourier transforms (FFT)[77] but modified according to the method of Mowrey[75] due to the L-shape grid considered; instead of two-dimensional FFT's in the entire rectangular grid, monodimensional FFT's are performed for each radial coordinate but only at points included in the L-shape domain. This requires the definition of n_{1L} and n_{2L}, the number of points which characterize the size of the small FFT's performed in R_1 and R_2 grids, respectively. Acceptable values for them are 112 for n_{1L} and 120 for n_{2L} in both calculations.

In bond coordinates there are many radial derivatives in the Hamiltonian to be evaluated, and it is crucial to reduce the number of Fourier transforms as much as possible. Thus, terms of the type $\partial/\partial R_i$ and $\partial^2/\partial R_i^2$, involve one direct and two inverse monodimensional Fourier transforms, and the evaluation of $\partial^2/\partial R_1\partial R_2$ would involve about two direct and two inverse Fourier transforms. That make a total number of ten monodimensional Fourier transforms. Collecting some of the transformations, this number can be reduced to only seven, which compares with the four required when using Jacobi coordinates within the L-shape method.

The action of the terms involving derivatives in α is evaluated through a discrete variable representation (DVR) transformation,[78–83] what reduces the procedure to a simple multiplication of a matrix by a vector.[78–83] In fact, the required number of matrix multiplications is only four (two for $\Omega'=\Omega$ and two for $\Omega'=\Omega\pm1$), while in the case of Jacobi coordinates there are only two multiplications (one for $\Omega'=\Omega$ and one for $\Omega'=\Omega\pm1$).

Therefore, the propagation of the wave packet in these bond coordinates is approximately a factor of 2 more expensive than the corresponding one using Jacobi coordinates. The efficiency of this method stems from the possible reduction in the number of points necessary to describe the region of the configuration space of interest. This fact depends strongly on the system under study, specially on the masses, and will be analyzed for the particular case of LiHF and its isotopomers.

C. Initial wave packet

The initial wave packet is placed in the asymptotic region where the interaction potential between the two reactants is zero. Reactant Jacobi coordinates are ideal to describe the eigenstates of the asymptotic Hamiltonian, which in the body-fixed frame defined before (see Fig. 1) take the form[44,50,84]

$$\phi^{E}_{JMvj\Omega_o p}=\left(\frac{\mu}{2\pi\hbar^2 k_{vj}}\right)^{1/2}\frac{\chi_{v,j}(r)}{r}\times\sum_{\Omega\geqslant 0}\frac{\mathcal{H}^{Jjp}_{\Omega_0\Omega}(k_{vj}R)}{R}W^{Jp}_{M\Omega}Y_{j\Omega}(\gamma,0)\rightarrow E=E_{vj}+\frac{\hbar^2k^2_{vj}}{2\mu} \tag{11}$$

corresponding to a total energy E, total angular momentum J, with projections M and Ω_0 on the space-fixed and body-fixed frames (the latter projection corresponding to $R\rightarrow\infty$) respectively, and a rovibrational state (v,j) of the diatomic fragment, with, $k_{vj}=\sqrt{2\mu(E-E_{vj})/\hbar^2}$. The functions $\mathcal{H}^{J}_{\Omega_0^{jp}\Omega}$ are *parity defined body-fixed Bessel functions*[84,44,50] defined as

$$\mathcal{H}^{Jjp}_{\Omega_0\Omega}=\frac{1}{\sqrt{1+\delta_{\Omega_0,0}}}\frac{1}{\sqrt{1+\delta_{\Omega,0}}}(\mathcal{H}^{Jj}_{\Omega_0\Omega}+p\times(-1)^J\mathcal{H}^{Jj}_{\Omega_0-\Omega}), \tag{12}$$

$$\mathcal{H}^{Jj}_{\Omega_0\Omega}=(-1)^{-\Omega_0-\Omega}\sum_l(-i)^l(2l+1)k_{vj}Rh^{(2)}_l(k_{vj}R)\times\begin{pmatrix} j & l & J\\ \Omega_0 & 0 & -\Omega_0\end{pmatrix}\begin{pmatrix} j & l & J\\ \Omega & 0 & -\Omega\end{pmatrix},$$

where $h^{(2)}_l$ is a spherical Bessel function of the third kind,[85] which asymptotically behaves as $h^{(2)}_l\sim_{R\rightarrow\infty}e^{-i(kR-l\pi/2)}/kR$. For $R\rightarrow\infty$, $\mathcal{H}^{Jj}_{\Omega_0\Omega}$ are zero if $\Omega\neq\Omega_0$ and the only one which remains, $\mathcal{H}^{Jj}_{\Omega_0\Omega_0}$, tends to $\exp(-ikR)$ (incoming wave). The lower the J value, the sooner the asymptotic behavior is reached.

The initial wave packet can be then defined as a superposition of these zero-order eigenstates of the form,

$$\Psi^{JMp}(t=0)=\int dEa(E)\phi^{E}_{JMvj\Omega_o p} \tag{13}$$

so that using Eq. (11) becomes

$$\Psi^{JMp}(t=0)=\frac{\chi_{v,j}(r)}{r}\int dEa(E)\left(\frac{\mu}{2\pi\hbar^2k_{vj}}\right)^{1/2}\times\sum_{\Omega\geqslant0}\frac{\mathcal{H}^{Jjp}_{\Omega_0\Omega}(k_{vj}R)}{R}W^{Jp}_{M\Omega}Y_{j\Omega}(\gamma,0). \tag{14}$$

As discussed above, for $R\rightarrow\infty$ the sum over Ω reduces to only one term with $\Omega=\Omega_0$, but as R becomes shorter the Coriolis coupling acts and the initial wave packet corresponds to a superposition of several Ω, analogous to Eq. (6), in which each coefficient has the form

$$\hat{\Phi}^{JMp}_{\Omega}(r,R,\gamma,t=0)=\chi_{v,j}(r)Y_{j\Omega}(\gamma,0)\int dEa(E)\times\left(\frac{\mu}{2\pi\hbar^2k_{vj}}\right)^{1/2}\mathcal{H}^{Jjp}_{\Omega_0^{jp}\Omega}(k_{vj}R), \tag{15}$$

where the only unknown is $a(E)$, which determine the initial conditions together with the quantum numbers (J,M,Ω_0,v,j).

To determine values for an acceptable $a(E)$ in the calculation, we do the following. For $\Omega=\Omega_0$ we choose a zero-order wave packet,

$$\chi_{vj}(r)Y_{j\Omega_0}(\gamma,0)G(R), \tag{16}$$

where $G(R)$ is a complex Gaussian function

$$G(R)=\left(\frac{2}{\pi\Gamma^2}\right)^{1/4}\exp\left[-\frac{(R-R_0)^2}{\Gamma^2}-i\mathcal{K}_0(R-R_0)\right] \tag{17}$$

centered at a convenient R_0 value such that the interaction between the reactants is negligible. $a(E)$ is then determined using Eq. (15) as

$$a(E)=\left(\frac{\mu}{2\pi\hbar^2k_{vj}}\right)^{1/2}\int k_{vj}Rh^{(2)*}_{l_{CS}}(k_{vj}R)G(R)dR, \tag{18}$$

where l_{CS} is the integer closest to l satisfying $l(l+1)=J(J+1)+j(j+1)-2\Omega_0^2$, so that the $\hat{\Phi}^{JMp}_{\Omega}(r,R,\gamma,t=0)$ coefficients with $\Omega\neq\Omega_0$ can be obtained using Eq. (15).

The initial wave packet thus obtained in reactant Jacobi coordinates must be transformed to bond coordinates (see Fig. 1) in which the propagation is performed as described above. Since the body-fixed frame is the same in the two sets of internal coordinates, the quantum number Ω remains the same, and imposing that the total wave packet is the same we get[50]

$$\Phi^{JMp}_{\Omega}(R_1,R_2,\alpha,t=0)=\left[\frac{R_2}{R}\hat{\Phi}^{JMp}_{\Omega}(r,R,\gamma,t=0)\right]_{(r,R,\gamma)\equiv(R_1,R_2,\alpha)} \tag{19}$$

with $r=R_1$, $R=\sqrt{R_2^2+q^2R_1^2-2qR_1R_2\cos\alpha}$ and $\cos\gamma=(R_2\cos\alpha-qR_1)/R$.

D. Final state analysis

The state-to-state energy resolved reaction probabilities are calculated using the Balint-Kurti *et al.* method.[40,86] For this purpose, the wave packet must be transformed to the product Jacobi coordinates $(r',R',\gamma',\theta',\phi',\chi')$. r' is the LiF internuclear distance, R' is the distance between the LiF center-of-mass and the H atom, γ' is the angle between these two vectors, and the Euler angles $(\theta',\ \phi',\ \chi')$ connect the new body-fixed and space-fixed frames (see Fig. 1). For product Jacobi coordinates we use the body-fixed frame in which the three atoms are in the $x-z$ body-fixed plane, as in the previous case, but now the body-fixed z-axis lies along $\mathbf{R}'$, i.e., the vector joining the LiF center of mass to the H atom.

Once the wave packet is transformed to produce Jacobi coordinates at each time step (what will be discussed below), the state-to-state reaction probabilities are obtained using[40,86]

$$P^{JMp}_{vj\Omega\to v'j'\Omega'}(E)=\frac{2\pi}{|a(E)|^2}\frac{k_{v'j'}}{\mu'}|A_{v'j'\Omega'}(E)|^2, \tag{20}$$

where $a(E)$ is defined in Eq. (18), $k_{v'j'}=\sqrt{2\mu'(E-E_{v'j'})/\hbar^2}$ (with $\mu'=m_1(m_0+m_2)/(m_0+m_1+m_2)$) and $A_{v'j'\Omega'}(E)$ is given by

$$A_{v'j'\Omega'}(E)=\frac{1}{2\pi}\sum_{\Omega''}\mathcal{H}^{Jjp}_{\Omega'\Omega''}(k_{v'j'}R'_\infty)\int_0^\infty dt e^{iEt/\hbar} \times\langle\chi_{v'j'}(r')Y_{j'\Omega''}(\gamma',0)|\tilde{\Phi}^{JMp}_{\Omega''}(r',R'_\infty,\gamma',t)\rangle, \tag{21}$$

where again the body-fixed Bessel functions are used to impose the correct asymptotic behavior at finite $R'\equiv R'_\infty$ distances, but in the product body-fixed frame.

To change the coordinates, from bond coordinates in the reactant body-fixed frame, used in the propagation, to product Jacobi coordinates in its associated body-fixed frame, used for the final analysis, some considerations must be taken into account that significantly reduce the procedure. First, the change of body-fixed frame corresponds to a rotation around the common y axis, which is perpendicular to the plane where the three atoms lie. Second, $r'\equiv R_2$, the LiF internuclear distance, and therefore, the transformation does not affect this coordinate. Finally, for the calculation of the state-to-state probabilities one only needs to evaluate the wave packet for $R'\equiv R'_\infty$. In addition, if the transformation is performed in several steps the procedure of changing the coordinates can be very efficient, and in the present work these steps are

(1) First the body-fixed frame is changed from reactant to product frames without changing the internal coordinates. Since the y-axis and y'-axis are the same, this transformation corresponds to a rotation around such axis.[73] The $\Phi^{JMp}_{\Omega'}(R_1,R_2,\alpha,t)$ coefficients in the product body fixed frame using well defined parity angular functions transform as

$$\Phi^{JMp}_{\Omega'}(R_1,R_2,\alpha,t)=\frac{1}{\sqrt{1+\delta_{\Omega',0}}}\sum_{\Omega\geqslant 0}\frac{1}{\sqrt{1+\delta_{\Omega,0}}}(d^J_{\Omega'\Omega}(\beta)+p(-1)^{J+\Omega}d^J_{\Omega'-\Omega}(\beta))\times\Phi^{JMp}_{\Omega}(R_1,R_2,\alpha,t), \tag{22}$$

where Ω is the total angular momentum projection on the reactant Jacobi body-fixed frame, while Ω' is the same but for the product Jacobi frame. The angle β is given by

$$\cos\beta=\frac{-qR_1^2-q'R_2^2+(1+qq')R_1R_2\cos\alpha}{R\sqrt{R_1^2+(q')^2R_2^2-2q'R_1R_2\cos\alpha}} \tag{23}$$

with $q'=\mu_2/m_0$, and $R=R(R_1,R_2,\alpha)$ given above.

(2) In the product body-fixed frame, the internal coordinates are partially transformed from (R_1,R_2,α) to $(r'\equiv R_2,\ R'=R'_\infty,\alpha)$, i.e., to the single value $R'=R'_\infty$ required to evaluate the state-to-state reaction probabilities. For this transformation we use a Fourier interpolation in R_1.[50]

(3) Finally, the wave packet is totally transformed to product Jacobi coordinates by an interpolation in the α angle which is performed using an expansion in associated Legendre functions to finally obtain the required $\tilde{\Phi}^{JMp}_{\Omega'}(r',R'_\infty,\gamma',t)$.

The procedure thus described becomes very efficient and the computational expense becomes negligible with respect to that of the propagation.

III. RESULTS AND DISCUSSION

A. Advantages of using bond coordinates

The use of spherical coordinates introduces singularities in the associated kinetic energy operator if any of the coordinates becomes undefined as it happens when radial coordinate becomes zero,[87] what would invalidate the use of the standard FFT algorithm for evaluating radial derivatives on a radial grid independently of the angular variables. Thus the efficiency of the method would be strongly reduced to avoid the problems associated to singularities, when they appear in the region of the configuration space of interest.

Some of the singularities are avoided because the potential become infinite when a distance between two atoms becomes zero. That is the case of R_1 and R_2 in bond coordinates and r or r' in reactant or product Jacobi coordinates. However, in Jacobi coordinates, R and R' describe the distance between an atom and the center-of-mass of a diatom, and when the diatom elongates, i.e., r or r' increases, the linear configuration with $R=0$ may occur. Such a situation is illustrated in Figs. 2, where the potential interaction is shown for LiHF and its isotopic variants in bond and reactant Jacobi coordinates. It is clearly seen that for LiDF and LiTF the $R=0$ value is energetically accessible for distances where the interaction potential between the products has not vanished.

Besides the singularity, the efficiency of using bond coordinates as compared to the use of Jacobi coordinates depends on the number of points of the grid required to converge the calculation in each set of coordinates. Assuming that the strong interaction region is reasonably well de-

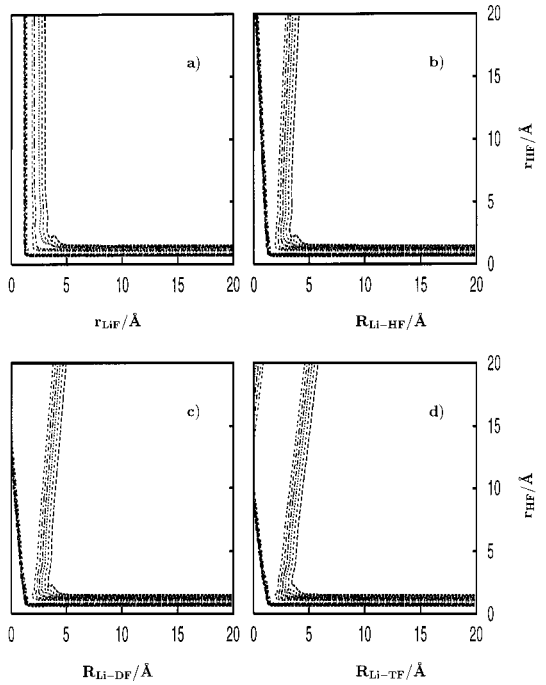

FIG. 2. Potential energy as a function of radial variables in (a) bond coordinates (being independent under isotopic substitution in this case) and reactant Jacobi coordinates for (b) LiHF, (c) LiDF, and (d) LiTF. The plot corresponds to the minimum of the potential as a function of the angular variable and a fixed value of radial variables. The contours are 0.5, 1, 1.5, 2, 2.5, and 3 eV with respect to the minimum of the well of isolated HF.

scribed by any of the coordinates considered, the question is how they describe the asymptotic regions where the analysis of the final states of products or reactants is performed. In Table II we show the error of the norm of the wave packets when represented in several coordinate sets. The wave packets, built as in Eq. (16), correspond to different states of the possible diatomic products, for the cases of LiHF, LiDF, and LiTF. The number of radial points in the three sets of coordinates are similar and the main factor governing the convergence of the norms is the number of points in the angular grid. In product Jacobi coordinates for LiHF three times more angular points than in any other set are needed to describe a wave packet in the reactant valley, and therefore this set is pretty badly adapted to describe the complete configuration space of interest at once. Reactant Jacobi coordinates and bond coordinates are similarly well adapted to describe both arrangement channels at the same time in the case of LiHF, because the center-of-mass of the HF is very close to the F atom. However, as the mass increases to LiDF and LiTF the number of angular points required also increases when using reactant Jacobi coordinates while remains essentially the same in bond coordinates.

Taking the case of LiF($v=0,j=30$) as an example, the number of angular points required when using bond coordinates is 40 for any of the isotopomers, while for reactant Jacobi coordinates is 50, for LiHF, 65 for LiDF, and 110 for LiTF. The advantages of using bond coordinates increases then with the mass. Moreover, the relative L-shape character of the grid considered is more favorable to bond coordinates as the mass of the satellite atoms approach that of the heavier central atom, as can be seen in Fig. 2.

In order to compare the efficiency of using bond coordinates versus reactant Jacobi coordinates we have performed the evaluation of $H\Psi$ 400 times in the two sets of coordinates for different isotopomers. While the radial grids used in the two coordinate representations are composed of the same total number of points, 440×462, n_{1L} and n_{2L} have been chosen according to the L-shapes observed in Figs. 2. The angular grid is composed by 40 points in bond coordinates, irrespective of the mass, and 50, 65, and 110 in reactant Jacobi coordinates for LiHF, LiDF, and LiTF, respectively. Taking as 100 arbitrary units the time required in bond coordinates, the calculation in reactant Jacobi coordinates takes 75, 125, and 300 arbitrary units for LiHF, LiDF, and LiTF, respectively. These numbers are only orientative about the relative efficiency since all the procedures depend on the particular computer used, libraries, etc. However they allow us to affirm that the relative efficiency of using bond coordinates increases with the mass, and the memory requirements decrease.

B. Application to Li+HF($v=0,1,j=0,J=0$)→LiF(v',j')+H

The Li+HF reaction presents a late barrier, located at long HF internuclear distances, and hence, the initial vibrational excitation produces a large enhancement of the reaction efficiency.[88,89] Total reaction probabilities and total reaction cross sections have been calculated in the CS approximation using reactant Jacobi coordinates[61,64] for several initial states of the reactants ($v=0$, 1, $j=0$, 1, 2, and 3). Such calculations show, as expected, that the reaction cross section for $v=1$ is about 10–50 times larger than that corresponding to $v=0$, even at the same total energies.[61,64] In this work we present state-to-state wave packet calculations for the Li+HF($v=0,1,j=0,J=0$)→LiF(v',j')+H reactive collision, using the GPES of Ref. 61 and the parameters listed in Table I. There are some previous quantum calculations on the state-to-state reaction probabilities of this reaction for $v=0$[52,60,62] but a quantitative comparison with the present results is not possible since all of them used a different GPES, that of Ref. 60. Nevertheless, the analogies in the dynamics in the two surfaces will be commented.

The total reaction probabilities for $v=0$ and 1 (with $J=j=0$), in Fig. 3, show the enhancement of reactivity with the vibrational excitation of HF. Such results are in perfect agreement with the total reaction probabilities calculated earlier using reactant Jacobi coordinates.[61,64] Moreover, in order to stress the good accuracy of the procedure, the Li+HF($v=0,j=0$)→LiF($v'=0,j'=0$ and 1)+H probabilities are compared in Fig. 4 with some recent results of Castillo[65] using the hyperspherical CC method,[90] showing a very good agreement even at low energies and in the vicinity of narrow resonances.

The total reaction probability for $v=0$ in Fig. 3 shows many resonances, especially at low energies, superimposed to an oscillating envelope. The narrow resonances are essentially due to the relatively deep well in the reactant valley as it was also interpreted in Ref. 60. The oscillating envelope is

TABLE II. Numerical errors in the square norms of wave packets of the form of Eq. (16), calculated using the three different sets of coordinates considered, using the same radial grids (similar to the ones for the $v=0$, $j=0$ propagation) and varying the number of points of the angular grid.

	Error in the norm in product Jacobi coordinates			Error in the norm in bond coordinates			Error in the norm in reactant Jacobi coordinates		
LiF(v,j)+H[a]	$n_{\gamma'}=32$	$n_{\gamma'}=40$	$n_{\gamma'}=50$	$n_{\alpha}=32$	$n_{\alpha}=40$	$n_{\alpha}=50$	$n_{\gamma}=32$	$n_{\gamma}=40$	$n_{\gamma}=50$
$v=0$, $j=0$	10^{-7}	10^{-7}	10^{-7}	10^{-7}	10^{-7}	10^{-7}	10^{-7}	10^{-7}	10^{-7}
$v=0$, $j=20$	10^{-7}	10^{-7}	10^{-7}	10^{-7}	10^{-7}	10^{-7}	10^{-5}	10^{-7}	10^{-7}
$v=0$, $j=25$	10^{-7}	10^{-7}	10^{-7}	10^{-7}	10^{-7}	10^{-7}	10^{-2}	10^{-7}	10^{-7}
$v=0$, $j=30$	10^{-7}	10^{-7}	10^{-7}	10^{-2}	10^{-7}	10^{-7}	10^{-2}	10^{-1}	10^{-7}
$v=5$, $j=0$	10^{-6}	10^{-6}	10^{-6}	10^{-6}	10^{-6}	10^{-6}	10^{-6}	10^{-6}	10^{-6}
$v=5$, $j=20$	10^{-6}	10^{-6}	10^{-6}	10^{-6}	10^{-6}	10^{-6}	10^{-5}	10^{-6}	10^{-6}
$v=5$, $j=25$	10^{-6}	10^{-6}	10^{-6}	10^{-6}	10^{-6}	10^{-6}	10^{-1}	10^{-6}	10^{-6}
$v=5$, $j=30$	10^{-6}	10^{-6}	10^{-6}	10^{-2}	10^{-6}	10^{-6}	10^{-1}	10^{-1}	10^{-6}
LiF(v,j)+D[a]	$n_{\gamma'}=32$	$n_{\gamma'}=40$	$n_{\gamma'}=65$	$n_{\alpha}=32$	$n_{\alpha}=40$	$n_{\alpha}=65$	$n_{\gamma}=32$	$n_{\gamma}=40$	$n_{\gamma}=65$
$v=5$, $j=0$	10^{-6}	10^{-6}	10^{-6}	10^{-6}	10^{-6}	10^{-6}	10^{-6}	10^{-6}	10^{-6}
$v=5$, $j=15$	10^{-6}	10^{-6}	10^{-6}	10^{-6}	10^{-6}	10^{-6}	10^{-3}	10^{-6}	10^{-6}
$v=5$, $j=20$	10^{-6}	10^{-6}	10^{-6}	10^{-6}	10^{-6}	10^{-6}	10^{-1}	10^{-3}	10^{-6}
$v=5$, $j=25$	10^{-6}	10^{-6}	10^{-6}	10^{-6}	10^{-6}	10^{-6}	10^{-3}	10^{-1}	10^{-2}
$v=5$, $j=32$	10^{-6}	10^{-6}	10^{-6}	10^{-2}	10^{-6}	10^{-6}	10^{-2}	10^{-2}	10^{-1}
LiF(v,j)+T[a]	$n_{\gamma'}=75$	$n_{\gamma'}=90$	$n_{\gamma'}=110$	$n_{\alpha}=75$	$n_{\alpha}=90$	$n_{\alpha}=110$	$n_{\gamma}=75$	$n_{\gamma}=90$	$n_{\gamma}=110$
$v=5$, $j=0$	10^{-6}	10^{-6}	10^{-6}	10^{-6}	10^{-6}	10^{-6}	10^{-6}	10^{-6}	10^{-6}
$v=5$, $j=15$	10^{-6}	10^{-6}	10^{-6}	10^{-6}	10^{-6}	10^{-6}	10^{-5}	10^{-6}	10^{-6}
$v=5$, $j=20$	10^{-6}	10^{-6}	10^{-6}	10^{-6}	10^{-6}	10^{-6}	10^{-5}	10^{-6}	10^{-6}
$v=5$, $j=25$	10^{-6}	10^{-6}	10^{-6}	10^{-6}	10^{-6}	10^{-6}	10^{-3}	10^{-5}	10^{-6}
$v=5$, $j=30$	10^{-6}	10^{-6}	10^{-6}	10^{-6}	10^{-6}	10^{-6}	10^{-2}	10^{-4}	10^{-6}
Li+HF(v,j)[b]	$n_{\gamma'}=32$	$n_{\gamma'}=70$	$n_{\gamma'}=130$	$n_{\alpha}=32$	$n_{\alpha}=70$	$n_{\alpha}=130$	$n_{\gamma}=32$	$n_{\gamma}=70$	$n_{\gamma}=130$
$v=0$, $j=0$	10^{-1}	10^{-3}	10^{-6}	10^{-7}	10^{-7}	10^{-7}	10^{-7}	10^{-7}	10^{-7}

[a]Wave packet located in the asymptotic region of the product channel.
[b]Wave packet located in the asymptotic region of the reactant channel.

attributed to broad resonances associated to the transition state;[64] at the saddle point the reaction path is approximately coincident with the HF stretch, and eliminating this degree of freedom bound state calculations were performed which yield eigenvalues approximately at the maxima of the envelope of the reaction probability for $v=0$. Such transition state resonances (TSR) were first calculated by Schatz and Kuppermann[91] for $H+H_2$ reactive collisions and since then have been the subject of an extensive work on this system and its isotopic variants.[30,92–96] These quantized transition state resonances have been used to interpret and analyze the reaction probabilities arising from accurate quantum scattering calculations for a wide variety of reactions.[97] The integral rate constant for $H+H_2$ collisions does not show any structure associated with such TSR, either experimentally[98] or theoretically,[94] due to the average on the partial waves that washes out such structures. However, for other systems such structures have been detected in the total reaction cross section, as in the case of $Ca(^1D)+HBr$.[99]

For Li+HF, Baer *et al.*[62] showed some peaks in the integral reaction cross section at low translational energies (below 0.12 eV) using the potential of Palmieri and Laganà.[100] They associated those structures to interference effects analogous to the Fraunhofer diffraction in optics. Later on, Zhang and co-workers using the GPES of Ref. 60, calculated the total reaction cross section for HF$(v=0,j=0)$, within the CS approach, and no structure was present.[101] More recently, using a new GPES (Ref. 61) Lara *et al.* obtained the reaction cross section for several initial states of the HF reactant.[64] For $v=0$, $j=0$ the integral cross section showed

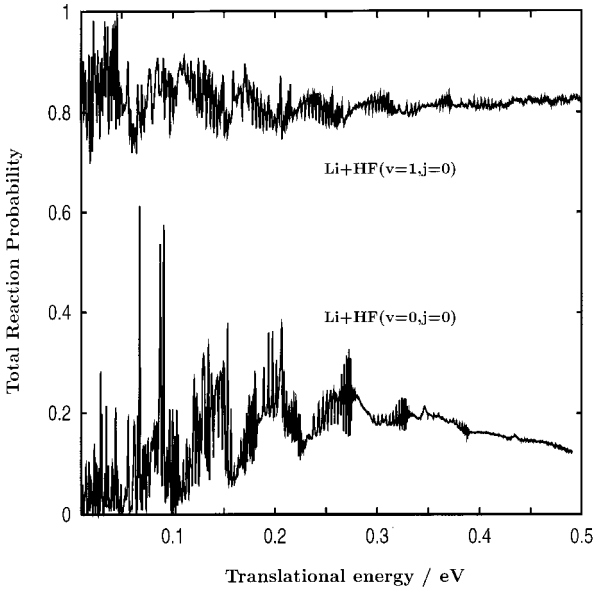

FIG. 3. Total reaction probabilities for Li+HF$(v=0,1,j=0,J=0)$.

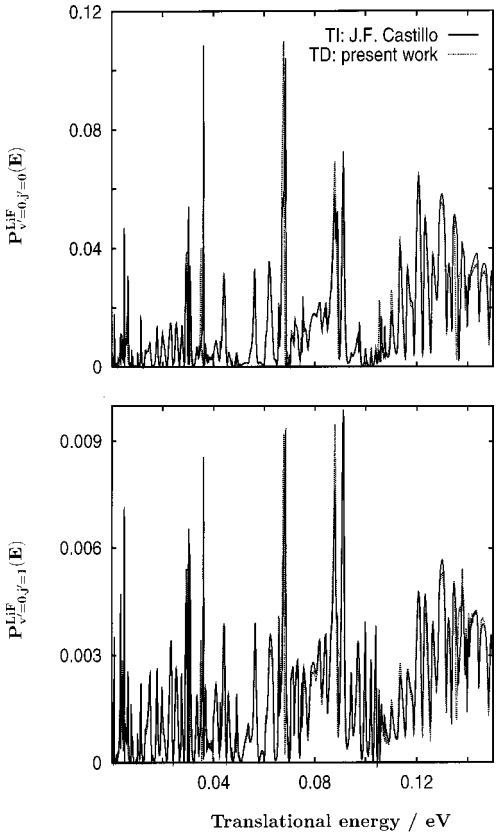

FIG. 4. State-to-state reaction probabilities for Li+HF($v=0,j=0,J=0$) $\rightarrow$H+LiF($v'=0,j'$) obtained in this work (dotted lines) compared to time-independent results of Castillo (Ref. 65); (a) for $j'=0$, (b) for $j'=1$.

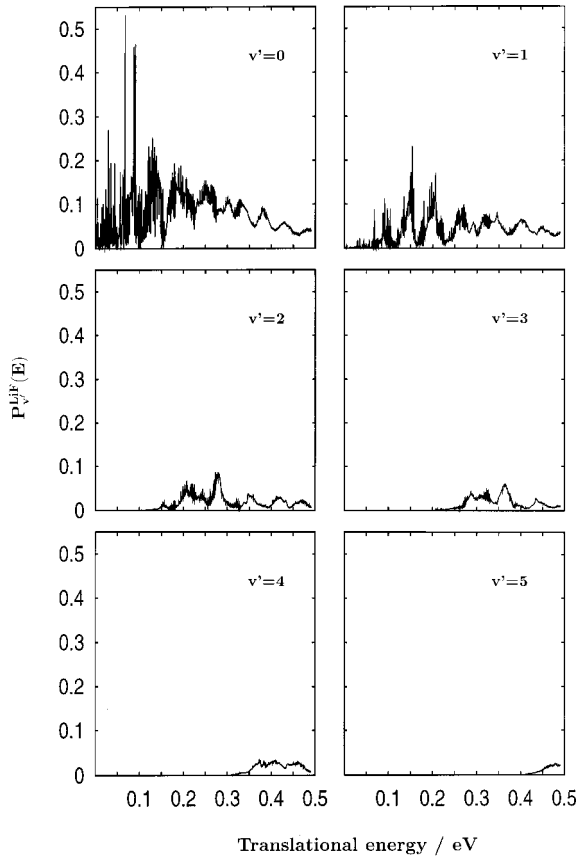

FIG. 5. Vibrationally resolved reaction probabilities for Li+HF($v=0,j=0,J=0$)$\rightarrow$H+LiF(v'). The separation between even and odd v' values has been made for clarity in the representation.

some oscillations attributed to TSR while for $v=0$, $j>0$ those oscillations disappear. After rotational average, however, the oscillations still remain appreciable. Although those oscillations are explained by quantum effects, recent quasiclassical trajectory calculations for HF($v=0$) showed also oscillations in the integral cross section,[102] but the results were not in quantitative agreement with the quantal results[64] using the same GPES.[61] Since those details in the total reaction cross section seem to be very sensitive to the potential energy surface, experimental measurements of these quantities would be of great help.

More detailed quantities not subject to the partial wave average, present more clear evidences of TSR. The state-to-state reaction probabilities obtained by Parker *et al.*[60] and Gögtas *et al.*[52] with the GPES of Ref. 60 showed oscillations. The vibrationally resolved reaction probabilities obtained in this work for Li+HF($v=0,j=0,J=0$) (state-to-state probabilities summed on final rotational quantum number), are shown in Fig. 5. The probabilities on each final v' show even more clearly the oscillations. At low translational energies (below 0.1 eV) the $v'=0$ is dominant. The $v'=1$ channel is open at zero translational energy, but it is not significant up to 0.1 eV. The first couple of maxima for $v'=1$ are approximately in phase with those of $v'=0$ and this is why the total reaction probabilities, in Fig. 3, show clear maxima around 0.08 and 0.14 eV. However, as energy increases the maxima associated to each probability, $v'=0$ and 1, dephase. Such effect, together with the opening of new v' channels, makes the oscillations disappear in the total reaction probability at high translational energies. As energy increases the density of transition state resonances increases. Therefore, it could be interesting to analyze if the maxima appearing for each v' are due to different TSR, each one favoring an individual v', or to some interference occurring in the product channel as a consequence of different kinetic energies for each LiF final state.

The Li+HF($v=0,j=0,J=0$)$\rightarrow$LiF($v'=0,j'$)+H reaction probabilities for individual final LiF($v'=0,j'$) rotational states, in Figs. 6, show a very distinct behavior for even and odd j'. It is notorious that the probabilities for $j'=1$ and 3 are nearly negligible, while those for $j'=0$ and 2 are really important and nearly equal. The situation for higher j' relax, but still there are common features among even or odd j', separately. Such a behavior means that even and odd j' are somehow decoupled. Moreover, this situation holds for other final vibrational states, v', and in Figs. 7 the reaction probabilities to form LiF($v'=2,j'$) are shown as an example.

The explanation of this curious result is again in the features of the transition state. The saddle point for the reaction is located at $R_1=1.301$ Å, $R_2=1.692$ Å, and $\alpha=71.4°$.[61] Transforming to product Jacobi coordinates, this means that $\gamma'=91.9°\approx\pi/2$. It can be assumed that the potential is locally quadratic as a function of γ' near the minimum placed at the saddle point, that is $V(\gamma')\approx V(\pi-\gamma')$,

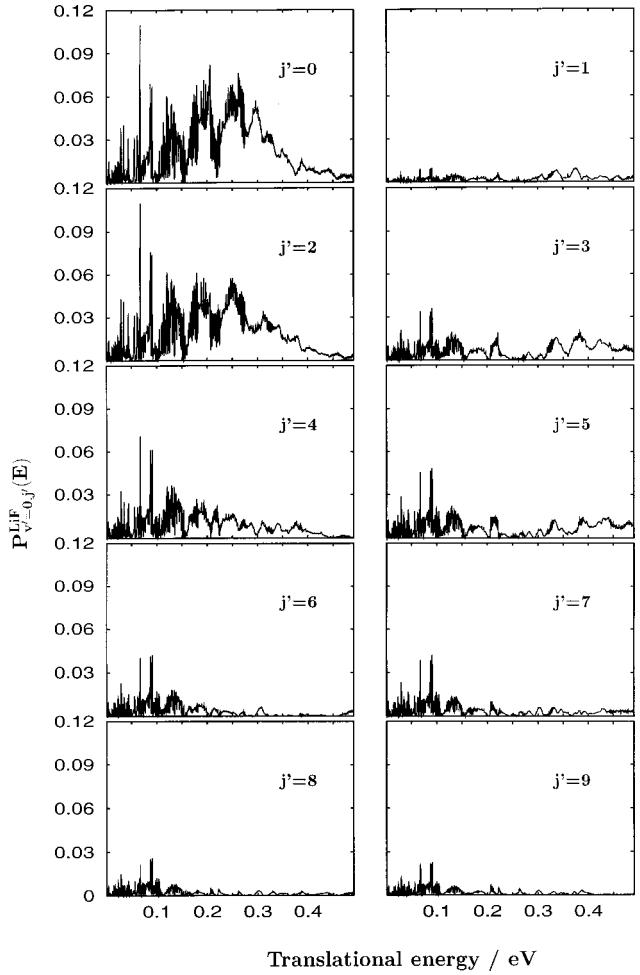

FIG. 6. State-to-state reaction probabilities for Li+HF($v=0,j=0,J=0$) $\rightarrow$H+LiF($v'=0,j'$).

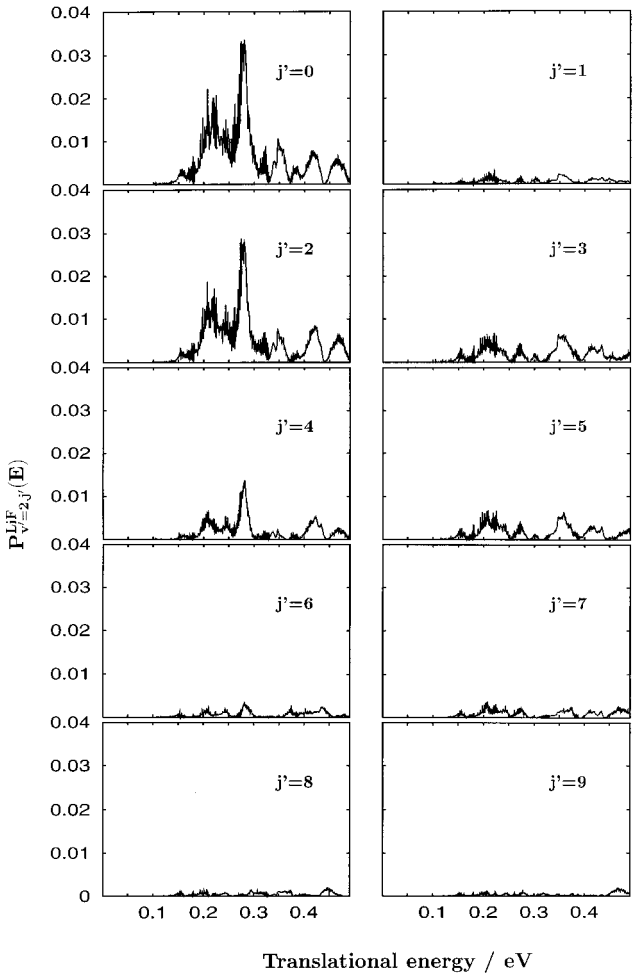

FIG. 7. State-to-state reaction probabilities for Li+HF($v=0,j=0,J=0$) $\rightarrow$H+LiF($v'=2,j'$).

for $\gamma' \approx \pi/2$ and the functions in γ' can be approximately separated as even or odd. Therefore, the TSR, located at the saddle point, should also show a quite good separation between even and odd functions in γ' when using product Jacobi coordinates. Once the system reacts, the light H atom is expected to fly apart relatively fast.[103] It can then be expected that the final rotational distribution of the LiF products show a ''memory'' of the structure of the TSR, which acts as a bottleneck, as it happens in direct photodissociation.[104] Therefore, the approximate separation between even and odd j' observed in Figs. 6 and 7 reflects the transition state structure which gates the reactive flux. Moreover, since the ground transition state should be an even solution in γ' it explains why even j' values have higher probability. As j' increases, the system explores angular regions far from the saddle point where the potential is not symmetric and therefore even and odd j' are not anymore decoupled. Thus, for high j' even and odd rotational states show a similar behavior. Also, since at high energy there are many TSR, each one with its own rotational structure, the separation between even and odd j' is cancelled even for low rotational states.

This simple and crude model used to explain the final rotational distribution is based on the location of the saddle point, that in fact is nearly identical for different GPES on this system. Göğtas *et al.*[52] also found that even and odd final rotational states of LiF products showed different behavior using the GPES of Ref. 60. The difference was however less notorious. The possible explanation is that in the GPES used[60] there is a relatively deep well in the product valley (which is very small in the GPES used in this work).[61] This well can complicate the dynamics in the product channel in such a way that the ''memory'' of the transition state resonance features is washed out.

The reaction dynamics for Li+HF($v=1$) is rather different. At these higher energies there are not threshold effects and the oscillations associated to TSR are less notorious than for $v=0$, as can be seen in Fig. 3 for the total reaction probability. Recent quasiclassical trajectory (QCT) calculations performed by Aoiz *et al.*[105] for Li+HF($v=1,j=0,1$) yielded a total reaction cross section in good agreement with previous quantum mechanical results[64] using the same GPES.[61] For $v=0$, however, there was not quantitative agreement between QCT[102] and quantum mechanical results.[61,64] The difference is that when a vibrational quantum is added to the HF reactant the reaction becomes considerably exoergic, having enough energy to overpass the barrier, and zero-point energy effects become negligible.

Moreover, the QCT differential cross sections are in agreement with experimental results, also in Ref. 105, showing the adequacy of the GPES[61] to describe the Li+HF reaction in the ground electronic state.

The total reaction cross section for $v=1$ shows a monotonous decrease with energy, with an energy dependence of $\approx E^{-2/3}$, both in quantum[64] and QCT[105] calculations. The total reaction cross section in this case does not show any trace of TSR. However, the reaction probability for $J=0$ already shows weak oscillations, which are more clearly seen in the vibrationally resolved state-to-state reaction probabilities, shown in Fig. 8 for several v' of LiF products. The amplitude of the oscillations for each individual v' is lower than for $v=0$, and they seem to be superimposed to a background. Also, for high v' and/or high translational energy the amplitude of the oscillations decreases. The weak oscillations occurring for different v' shift with respect to each other as energy increases, what can also explain their disappearance in the total reaction probability. Because of the large energy available, the final vibrational excitation of LiF fragments is distributed among many v' states. At low energy, low v' states are dominant. However, at higher energy, there is a population inversion, higher v' becoming more important, so that around 0.45 eV of translational energy, $v'=3$ is the largest one.

The rotational distribution of LiF products for $v=1$, see Fig. 9, is spread over a wide range of j' with the maximum located for $10 \leqslant j' \leqslant 20$, and with no particular difference between even and odd j' values. This is in contrast with the rotational distributions obtained for $v=0$, in Figs. 6 and 7, which are peaked at low j' values, decreasing very rapidly with increasing j', with a clear separation between even and odd j'. The reaction probabilities for each individual (v',j') state in Fig. 9 show a clear oscillatory behavior, what can be considered as an indication that they are mediated by TSR. The reason for the decrease of the oscillations in the total and vibrationally resolved reaction probabilities is the presence of many TSR, placed at different energies, what washes out the oscillations. The presence of many resonances somehow removes the specific rotational state distribution found for the $v=0$ case, for which only a single or few resonances are involved. There is an extraordinary similarity among the oscillation of the reaction probabilities for $j' \geqslant 21$, possibly because their appearance is mediated by the same TSR.

Considering the total available energy, the average values of the vibrational and rotational energy fractions for $v=0$ and 1 are quite similar, as can be seen in Fig. 10. The main differences are the structures associated with TSR in the $v=0$ case. For the two cases studied, the final vibrational energy of the products is not very important, $f_v \approx 20\%$ of the total energy, as it is expected in the presence of a late barrier.[106] This value is very close to the QCT results obtained by Aoiz *et al.*[105] of $f_v=20.6\%$ and 23% obtained for $v=1$ at translational energies of 0.231 and 0.416 eV, respectively. The rotational fraction f_R obtained in this work for $v=1$ is $f_R \approx 5\%$, while in the QCT calculations[105] this fraction is about 36%. This apparent discrepancy can be simply explained. In the present results only $J=0$ is considered while in the QCT ones all possible J's are included. Since this reaction corresponds to the heavy–heavy–light case, it is expected that l (the orbital angular momentum of the Li atom with respect to HF) is transformed to rotational excitation of the LiF products, j'. Therefore, the rotational energy fraction will increase when performing the partial waves average (considering higher J values). Assuming the QCT values to be the correct ones, these results are in good agreement with the partial angular constraint model by Bonnet and Rayez[107,108] applied to Li+HF collisions which yields $f_T \approx 42\%$ and $f_v \approx 20\%$.

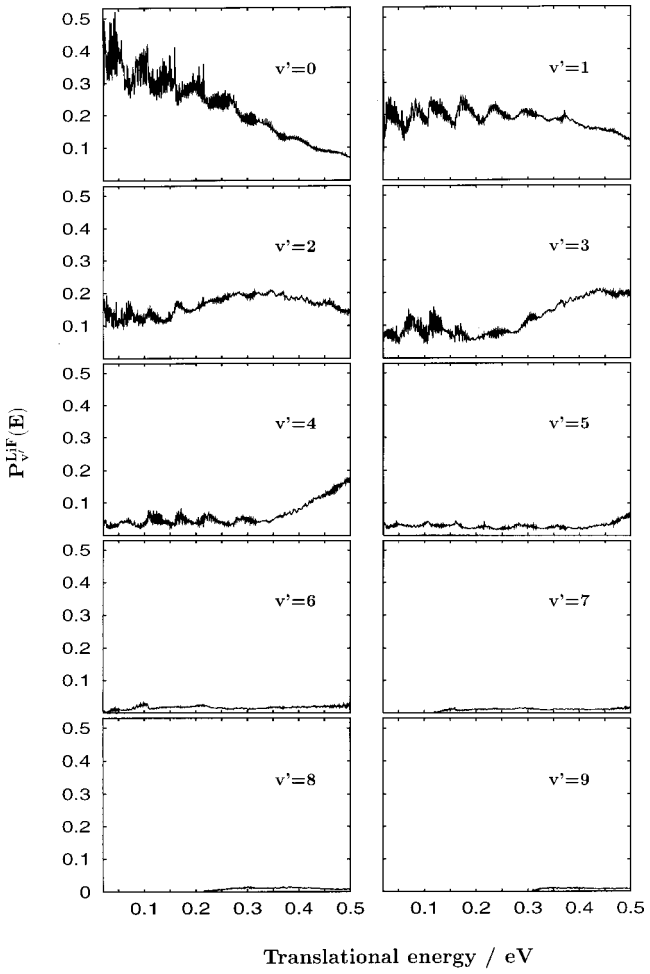

FIG. 8. Vibrationally resolved reaction probabilities for Li+HF($v=1,j=0,J=0$)→H+LiF(v').

IV. CONCLUSIONS

In this work we have presented a time-dependent method to evaluate state-to-state reaction probabilities, based on the use of bond coordinates. The use of these coordinates avoids the problems associated with the singularities of the radial kinetic terms, which may be present when using a set of Jacobi coordinates to describe the complete configuration space especially for long range interactions. The action of the Hamiltonian on a wave packet represented in grid in bond coordinates is approximately twice as expensive as using Jacobi coordinates. However, bond coordinates may require less number of points to reach convergence than the use of a particular set of Jacobi coordinates, saving time and memory

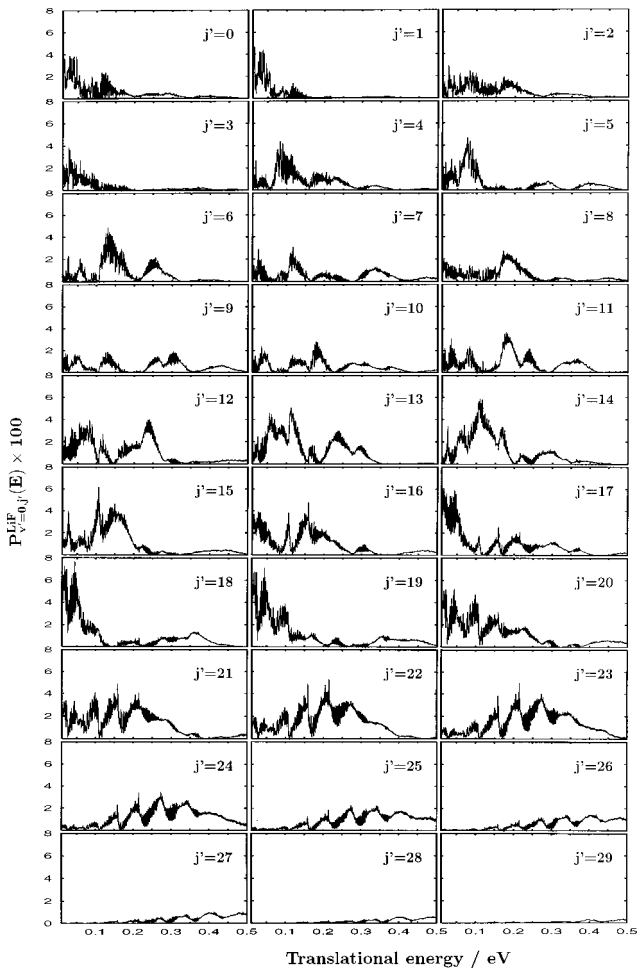

FIG. 9. State-to-state reaction probabilities for Li+HF($v=1,j=0,J=0$) $\rightarrow$H+LiF($v'=0,j'$).

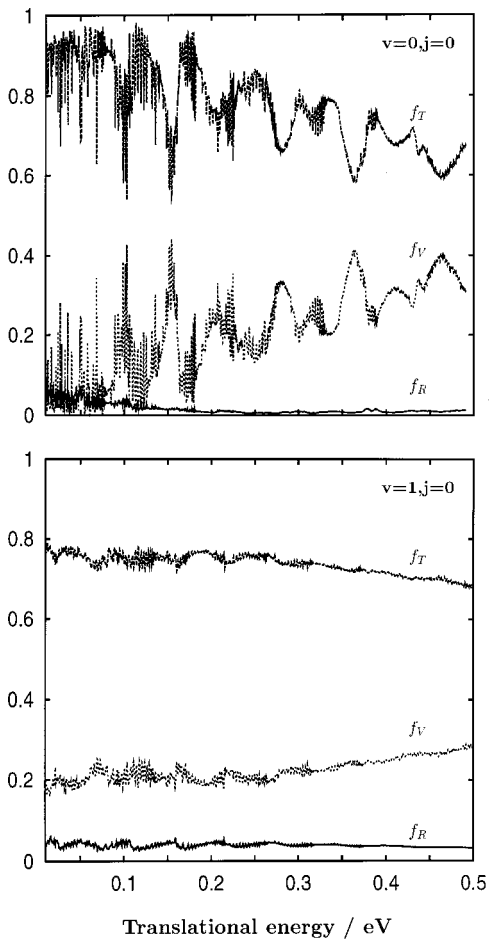

FIG. 10. Average values of translational, vibrational, and rotational energy fractions for the LiF(v',j') products; (a) Li+HF($v=0,j=0,J=0$); (b) Li+HF($v=1,j=0,J=0$).

requirements. Although, for the case of LiHF the number of points needed in reactant Jacobi coordinates is very similar to that in bond coordinates, as the mass of the hydrogen isotopes increases the number of points also increases when using reactant Jacobi coordinates while in bond coordinates this number of points remains almost unchanged. Thus, the use of bond coordinates becomes clearly more efficient for LiDF and LiTF, both in time and in memory requirements. In addition, the domain of interest of the configuration space remains essentially L-shaped independently of the masses, while in Jacobi coordinates its shape may strongly differ from such situations as the masses of the satellite atoms approach that of the central atom. As a consequence, the use of the L-shape method of Mowrey[75] improves the relative efficiency of the use of bond coordinates as compared to Jacobi coordinates for LiDF and LiTF. This gradual increase of the efficiency (because of the number of points and the L-shape domain) with the mass allows us to conclude that the method presented in this work may be very efficient as the mass of the satellite atoms increases. Moreover, for symmetric reactions, as $AB+A\rightarrow A+BA$, bond coordinates may be particularly interesting to take advantage of the symmetry. Of course, the best efficiency would be obtained by separating the propagation for the different arrangement channels[50–56] since the representation of the wave packet is done in the best coordinate set in each region. The main problem resides in the lost of accuracy when the wave packet spreads over a large region due to low kinetic energy and narrow resonances as it is the case of LiHF studied here. A more detailed analysis of the accuracy in using such methods is now being done.

The method is applied to Li+HF($v=0,1,j=0,J=0$) reactive collisions using the GPES of Ref. 61. The accuracy of the method is very good when compared with recent time-independent hyperspherical calculations in this system performed recently by Castillo,[65] even at low translational energies and for narrow resonances. The use of a well adapted body-fixed frame, the reactant Jacobi frame in the present case, is also described and its adequacy for the Li+HF collision is now being checked.

The final vibrational state population of the LiF products for $v=0$ shows oscillations with energy which are interpreted by the presence of TSR that drive the reaction flux. Also, the final rotational state population of LiF products for the case $v=0$ shows a net distinction between even and odd j' values which is interpreted by the topology of the saddle point for the reaction. The rotational state population is rather cold, being located at $j'=0$ and 2, decreasing rapidly with increasing j'.

For $v=1$ there is an important increase in the reaction

probability because this system shows a late barrier.[61,64] As a consequence of the higher energies, zero-point energy and threshold effects are less important and recent QCT calculations[105] are in good agreement with previous quantum calculations,[64] while for $v=0$ this is not the case. The final state distributions, both vibrational and rotational ones, are rather spread as a consequence of the higher energies involved, as compared to the $v=0$ case. Although the alternation between even and odd j' values is absent in this case, traces of a mechanism mediated by a multitude of TSR keep on existing.

ACKNOWLEDGMENTS

We want to stress our acknowledgment to Jesús F. Castillo for sharing with us his results, that allows us to check the accuracy of the method presented in this work. Also we thank F. J. Aoiz and E. Verdasco for providing us with a preprint prior to its publication. This work has been supported by DGICYT (Ministerio de Educación y Ciencia, Spain) under Grant Nos. PB97-0027 and PB95-0071, and by the European TMR network Contract No. ERBFMRX-CT96-0088. M. L. also thanks the Comunidad Autónoma de Madrid for a Grant. We also want to acknowledge DGICYT and CIEMAT for the use of a CRAY-J90.

[1] C. B. Moore and I. W. M. Smith, J. Phys. Chem. **100**, 12848 (1996).
[2] G. C. Schatz, J. Phys. Chem. **100**, 12839 (1996).
[3] P. L. Houston, J. Phys. Chem. **100**, 12757 (1996).
[4] L. Schneider, K. Seekamp-Rahn, J. Borkowski, E. Wrede, K. H. Welge, F. J. Aoiz, L. Bañares, M. J. D'Mello, V. J. Herrero, V. Sáez Rábanos, and R. E. Wyatt, Science **269**, 207 (1995).
[5] C. Maltz, N. D. Weinstein, and D. R. Herschbach, Mol. Phys. **24**, 133 (1972).
[6] D. S. Y. Hsu, N. D. Weinstein, and D. R. Herschbach, Mol. Phys. **29**, 257 (1975).
[7] G. M. McClelland and D. R. Herschbach, J. Phys. Chem. **83**, 1445 (1979).
[8] J. D. Barnwell, J. G. Loeser, and D. R. Herschbach, J. Phys. Chem. **87**, 2781 (1983).
[9] A. J. Orr-Ewing and R. N. Zare, Annu. Rev. Phys. Chem. **45**, 315 (1994).
[10] H. J. Loesch, Annu. Rev. Phys. Chem. **46**, 555 (1995).
[11] Special issue, J. Phys. Chem. **99**, 13569 (1995).
[12] Special issue, J. Phys. Chem. **101**, 7461 (1997).
[13] M. P. de Miranda and D. C. Clary, J. Chem. Phys. **106**, 4509 (1997).
[14] M. P. de Miranda, D. C. Clary, J. F. Castillo, and D. E. Manolopoulos, J. Chem. Phys. **108**, 3142 (1998).
[15] M. P. de Miranda, F. J. Aoiz, L. Bañares, and V. Sáez Rábanos, J. Chem. Phys. **111**, 5368 (1999).
[16] H. Nakamura, Annu. Rev. Phys. Chem. **48**, 299 (1997).
[17] A. Kuppermann and P. G. Hipes, J. Chem. Phys. **84**, 5962 (1986).
[18] P. G. Hipes and A. Kuppermann, Chem. Phys. Lett. **133**, 1 (1987).
[19] R. T. Pack and G. A. Parker, J. Chem. Phys. **87**, 3888 (1987).
[20] G. C. Schatz, Chem. Phys. Lett. **150**, 92 (1988).
[21] R. T. Pack and G. A. Parker, J. Chem. Phys. **90**, 3511 (1989).
[22] T. J. Park and J. C. Light, J. Chem. Phys. **91**, 974 (1989).
[23] J. M. Launay and M. Le Dourneuf, Chem. Phys. Lett. **163**, 178 (1989).
[24] B. Lepetit and J. M. Launay, J. Chem. Phys. **95**, 5159 (1991).
[25] V. Aquilanti, S. Cavalli, and D. De Fazio, J. Chem. Phys. **109**, 3792 (1998).
[26] V. Aquilanti, S. Cavalli, D. De Fazio, A. Volpi, A. Aguilar, X. Giménez, and J. Lucas, J. Chem. Phys. **109**, 3805 (1998).
[27] K. Haug, D. W. Schwenke, Y. Shima, D. G. Truhlar, J. Z. H. Zhang, and D. J. Kouri, J. Phys. Chem. **90**, 6757 (1986).
[28] J. Z. H. Zhang and W. H. Miller, Chem. Phys. Lett. **140**, 329 (1987).
[29] D. E. Manolopoulos and R. E. Wyat, Chem. Phys. Lett. **152**, 23 (1988).
[30] J. Z. H. Zhang and W. H. Miller, J. Chem. Phys. **91**, 1528 (1989).
[31] D. G. Truhlar, D. W. Schwenke, and D. J. Kouri, J. Phys. Chem. **94**, 7346 (1990).
[32] D. Neuhauser and M. Baer, J. Chem. Phys. **92**, 3419 (1990).
[33] D. Neuhauser and M. Baer, J. Chem. Phys. **91**, 4651 (1989).
[34] C. Leforestier and R. Wyatt, J. Chem. Phys. **78**, 2334 (1983).
[35] R. Kosloff and D. Kosloff, J. Comput. Phys. **63**, 363 (1986).
[36] R. Heather and H. Metiu, J. Chem. Phys. **86**, 5009 (1987).
[37] P. Pernot and W. A. Lester, Jr., Int. J. Quantum Chem. **40**, 577 (1991).
[38] K. C. Kulander and E. J. Heller, J. Chem. Phys. **69**, 2439 (1978).
[39] Y. Sun, R. C. Mowrey, and D. J. Kouri, J. Chem. Phys. **87**, 339 (1987).
[40] G. G. Balint-Kurti, R. N. Dixon, and C. C. Marston, J. Chem. Soc., Faraday Trans. **86**, 1741 (1990).
[41] D. J. Tannor and D. E. Weeks, J. Chem. Phys. **98**, 3884 (1993).
[42] D. H. Zhang, Q. Wu, and J. Z. H. Zhang, J. Chem. Phys. **102**, 124 (1995).
[43] J. Dai and J. Z. H. Zhang, J. Phys. Chem. **100**, 6898 (1996).
[44] Y. Sun, R. S. Judson, and D. J. Kouri, J. Chem. Phys. **90**, 241 (1989).
[45] W. H. Miller, J. Chem. Phys. **61**, 1823 (1974).
[46] D. Neuhauser, J. Chem. Phys. **93**, 7836 (1990).
[47] S. K. Gray and G. G. Balint-Kurti, J. Chem. Phys. **108**, 950 (1998).
[48] D. H. Zhang and J. C. Light, J. Chem. Phys. **104**, 4544 (1996).
[49] W. Zhu, J. Dai, J. Z. H. Zhang, and D. H. Zhang, J. Chem. Phys. **105**, 4881 (1996).
[50] R. S. Judson, D. J. Kouri, D. Neuhauser, and M. Baer, Phys. Rev. A **42**, 351 (1990).
[51] D. Neuhauser, M. Baer, R. S. Judson, and D. J. Kouri, J. Chem. Phys. **93**, 312 (1990).
[52] F. Gögtas, G. G. Balint-Kurti, and A. R. Offer, J. Chem. Phys. **104**, 7927 (1996).
[53] T. Peng and J. Z. H. Zhang, J. Chem. Phys. **105**, 6072 (1996).
[54] W. Zhu, T. Peng, and J. Z. H. Zhang, J. Chem. Phys. **106**, 1742 (1997).
[55] J. Dai and J. Z. H. Zhang, J. Chem. Soc., Faraday Trans. **93**, 699 (1997).
[56] S. C. Althorpe, D. J. Kouri, and D. K. Hoffman, J. Chem. Phys. **107**, 7816 (1997).
[57] G. D. Billing and N. Marković, J. Chem. Phys. **99**, 2674 (1993).
[58] N. Marković and G. D. Billing, J. Chem. Phys. **100**, 1085 (1994).
[59] B. Lepetit, J. M. Launay, and M. Le Dourneuf, Chem. Phys. **106**, 103 (1986).
[60] G. A. Parker, A. Laganà, S. Crocchianti, and R. T. Pack, J. Chem. Phys. **102**, 1238 (1995).
[61] A. Aguado, M. Paniagua, M. Lara, and O. Roncero, J. Chem. Phys. **107**, 10085 (1997).
[62] M. Baer, I. Last, and H. J. Loesch, J. Chem. Phys. **101**, 9648 (1994).
[63] A. Aguado, M. Paniagua, M. Lara, and O. Roncero, J. Chem. Phys. **106**, 1013 (1997).
[64] M. Lara, A. Aguado, O. Roncero, and M. Paniagua, J. Chem. Phys. **109**, 9391 (1998).
[65] J. F. Castillo (unpublished results).
[66] S. Carter and N. C. Handy, Mol. Phys. **47**, 1445 (1982).
[67] S. Carter, N. C. Handy, and B. T. Sutcliffe, Mol. Phys. **49**, 745 (1983).
[68] S. Carter and N. C. Handy, Comput. Phys. Rep. **5**, 117 (1986).
[69] N. C. Handy, Mol. Phys. **61**, 207 (1987).
[70] J. Makarewicz, J. Phys. B **21**, 1803 (1988).
[71] B. T. Sutcliffe and J. Tennyson, Mol. Phys. **58**, 1053 (1986).
[72] B. T. Sutcliffe and J. Tennyson, Int. J. Quantum Chem. **39**, 183 (1991).
[73] R. N. Zare, *Angular Momentum* (Wiley, New York, 1988).
[74] H. Tal-Ezer and R. Kosloff, J. Chem. Phys. **81**, 3967 (1984).
[75] R. C. Mowrey, J. Chem. Phys. **94**, 7098 (1991).
[76] D. H. Zhang and J. Z. H. Zhang, J. Chem. Phys. **101**, 1146 (1994).
[77] R. Kosloff, J. Phys. Chem. **92**, 2087 (1988).
[78] J. C. Light, I. P. Hamilton, and J. V. Lill, J. Chem. Phys. **82**, 1400 (1985).
[79] A. C. Peet and W. Yang, J. Chem. Phys. **91**, 6598 (1989).
[80] J. T. Muckerman, Chem. Phys. Lett. **173**, 200 (1990).
[81] G. C. Corey, J. W. Tromp, and D. Lemoine, in *Numerical Grid Methods and Their Application to the Schrödinger Equation*, edited by C. Cerjan (Kluwer Academic, New York, 1993), p. 1.
[82] O. A. Sharafeddin and J. C. Light, J. Chem. Phys. **102**, 3622 (1995).
[83] O. Roncero, D. Caloto, K. C. Janda, and N. Halberstadt, J. Chem. Phys. **107**, 1406 (1997).
[84] Y. Sun, R. S. Judson, and D. J. Kouri, J. Chem. Phys. **65**, 226 (1976).
[85] M. Abramowitz and I. A. Stegun, *Handbook of Mathematical Functions* (Dover, New York, 1972).
[86] G. G. Balint-Kurti, F. Gögtas, S. P. Mort, A. R. Offer, A. Laganà, and O. Gervasi, J. Chem. Phys. **99**, 9567 (1993).
[87] M. J. Bramley, J. W. Tromp, T. Carrington, Jr., and G. C. Corey, J. Chem. Phys. **100**, 6175 (1994).
[88] J. C. Polanyi and W. H. Wong, J. Chem. Phys. **51**, 1439 (1969).

[89] M. H. Mok and J. C. Polanyi, J. Chem. Phys. **51**, 1451 (1969).
[90] J. F. Castillo, D. E. Manolopoulos, K. Stark, and H.-J. Werner, J. Chem. Phys. **104**, 6531 (1996).
[91] G. C. Schatz and A. Kuppermann, Phys. Rev. Lett. **35**, 1266 (1975).
[92] G. C. Schatz, Chem. Phys. Lett. **94**, 183 (1983).
[93] S. A. Cuccaro, P. G. Hipes, and A. Kuppermann, Chem. Phys. Lett. **157**, 440 (1989).
[94] W. H. Miller, Annu. Rev. Phys. Chem. **41**, 245 (1990).
[95] D. C. Chatfield, R. S. Friedman, D. W. Schwenke, and D. G. Truhlar, J. Phys. Chem. **96**, 2414 (1992).
[96] R. T. Skodje, R. Sadeghi, H. Köppel, and J. L. Krause, J. Chem. Phys. **101**, 1725 (1994).
[97] D. G. Truhlar, B. C. Garret, and S. J. Klippenstein, J. Phys. Chem. **100**, 12771 (1996), and references therein.
[98] D. A. V. Kliner, D. E. Adelman, and R. N. Zare, J. Chem. Phys. **94**, 1069 (1991).
[99] M. Garay Salazar, A. González-Ureña, and G. Roberts, Isr. J. Chem. **37**, 353 (1997).
[100] P. Palmieri and A. Laganá, J. Chem. Phys. **91**, 7303 (1989).
[101] W. Zhu, D. Wang, and J. Z. H. Zhang, Theor. Chem. Acc. **96**, 31 (1997).
[102] F. J. Aoiz, M. T. Martínez, M. Menéndez, V. Sáez Rábanos, and E. Verdasco, Chem. Phys. Lett. **299**, 25 (1999).
[103] M. Paniagua, A. Aguado, M. Lara, and O. Roncero, J. Chem. Phys. **111**, 6712 (1999).
[104] R. Schinke, *Photodissociation Dynamics, Spectroscopy, and Fragmentation of Small Molecules* (Cambridge University Press, Cambridge, 1993).
[105] F. J. Aoiz, E. Verdasco, V. Sáez-Rabanos, H. J. Loesch, M. Menéndez, and F. Stienkemeier, Phys. Chem. Chem. Phys. **2**, 541 (2000).
[106] R. D. Levine and R. B. Bernstein, *Molecular Reaction Dynamics and Chemical Reactivity* (Oxford University Press, Oxford, 1987).
[107] L. Bonnet and J. C. Rayez, J. Chem. Phys. **102**, 9512 (1995).
[108] L. Bonnet and J. C. Rayez, Phys. Chem. Chem. Phys. **1**, 2383 (1999).